Chiral Co(II) Metal−Organic Framework in the Heterogeneous Catalytic Oxidation of Alkenes under Aerobic and Anaerobic Conditions

Giulia Tuci,[†] Giuliano Giambastiani,[†,‡] Stephanie Kwon,[§] Peter C. Stair,[⊥] Randall Q. Snurr,[§] and Andrea Rossin*[,†,‡]

[†]Consiglio Nazionale delle Ricerche, Istituto di Chimica dei Composti Organometallici (ICCOM-CNR), Via Madonna del Piano 10, 50019 Sesto Fiorentino (Firenze), Italy

[‡]Consorzio Interuniversitario per la Scienza e Tecnologia dei Materiali (INSTM), Via G. Giusti 9, 50121 Firenze, Italy

[§]Department of Chemical and Biological Engineering, [⊥]Department of Chemistry, Northwestern University, 2145 Sheridan Road, Evanston, Illinois 60208, United States

Ⓢ Supporting Information

ABSTRACT: The chiral Co(II) MOF $[Co(L\text{-}RR)(H_2O)\cdot H_2O]_\infty$ [**1**; L-*RR* = (*R*,*R*)-thiazolidine-2,4-dicarboxylate] has been exploited in the catalytic oxidation of different alkenes (cyclohexene, (*Z*)-cyclooctene, 1-octene) using either *tert*-butyl hydroperoxide (*t*BuOOH) or molecular oxygen (O_2) as oxidants. Different chemoselectivities are observed, both substrate- and oxidant-dependent. A moderate enantioselectivity is also obtained in the case of prochiral precursors, revealing the chiral induction ability of the optically pure metal environment. The interaction of O_2 with the exposed metal sites in **1** (after material preactivation and consequent removal of the coordinated aquo ligand) has been studied through TPD-MS analysis combined with DFT calculations, with the aim of probing effective oxygen uptake by the heterogeneous catalyst and unraveling the nature of the active species in the catalytic oxidation process under aerobic conditions. Theoretical results indicate the presence of an η^1-superoxo species at the cobalt center, with concomitant Co(II) ↔ Co(III) oxidation. Finally, the experimental estimation of the O_2 adsorption enthalpy is found to be in good agreement with the calculated binding energy.

KEYWORDS: metal−organic frameworks, cobalt (II), alkene oxidation, heterogeneous catalysis, DFT calculations, dioxygen activation
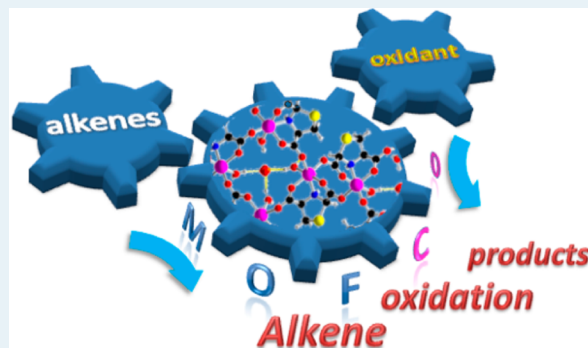
INTRODUCTION

The extremely high degree of freedom in the structural design of metal−organic frameworks (MOFs), achieved through a virtually infinite combination of inorganic secondary building units (SBUs) and organic linkers, opens new perspectives in the practical application of this class of materials. Thus, in addition to the initial exploitation of MOFs for gas storage purposes,[1] in the recent literature, more diversified applications have started to appear, spanning from separation and purification of gas mixtures[2] to luminescence,[3] ion sensing,[4] drug delivery,[5] and heterogeneous catalysis.[6] The employment of MOFs as catalysts for selected chemical transformations relies on the presence of catalytically active sites within their 3D networks. Transition metals, in particular, are good candidates for the activation of small molecules, which can coordinate to a vacant site within the metal's coordination sphere (the basic principle of homogeneous catalysis performed by transition metal organometallics).

In some MOFs, empty sites on the inorganic SBU can be generated through the simple removal of small neutral ligands from the metal coordination environment of the "unactivated" material (mostly H_2O, when operating under hydrothermal synthetic conditions; pure water or aqueous binary mixtures are the solvents of choice par excellence for MOF synthesis). The preactivation of the material is expected to create open metal sites potentially available for promoting catalysis while keeping the framework crystalline texture intact. In addition, the heterogeneous nature of a MOF can be very useful to separate the catalyst from the products of interest; recover it after simple filtration procedures; and finally, regenerate it for successive catalytic runs.

One industrially important reaction is the selective oxidation of hydrocarbons to higher-value chemical feedstocks.[7] Traditional catalytic procedures make use of polluting oxidizing agents (such as MnO_2 or CrO_3) that are environmentally unfriendly and difficult to recycle. Thus, in recent years, the

search for greener processes that could work with more benign oxidants has grown considerably. Among them, organic peroxides (R—OOH; R = alkyl chain), hydrogen peroxide (H_2O_2), and dioxygen (O_2) are the most popular.

Several examples of MOF-catalyzed hydrocarbon oxidation reactions using peroxides or dioxygen as oxidizing agents have appeared in the literature, exploiting metals coming from the first transition 3d series, such as chromium,[8] manganese,[9] iron,[10] and copper,[11] combined with assorted organic spacers. Cobalt, in particular, has been shown to be well-performing in olefin oxidation by organic peroxides or dioxygen with satisfactory activity and (chemo)selectivity under mild reaction conditions.[12] The main reaction products strongly depend on the nature of the oxidant and the presence of auxiliary radical initiators, such as N-hydroxyphtalimide (NHPI). If the heterogeneous catalyst of choice is optically active (because either it contains a chiral organic spacer or it bears optically active catalytic single sites embedded into the crystal lattice), enantioselective catalysis is also achievable.[13] Some of us have recently prepared and characterized a chiral Co(II) MOF based on an optically pure thiazolidine dicarboxylate ligand: $[Co(L\text{-}RR)(H_2O)\cdot H_2O]_\infty$ [1; L-RR = (R,R)-thiazolidine-2,4-dicarboxylate, Figure 1].[14] The Co(II) coordination sphere contains one
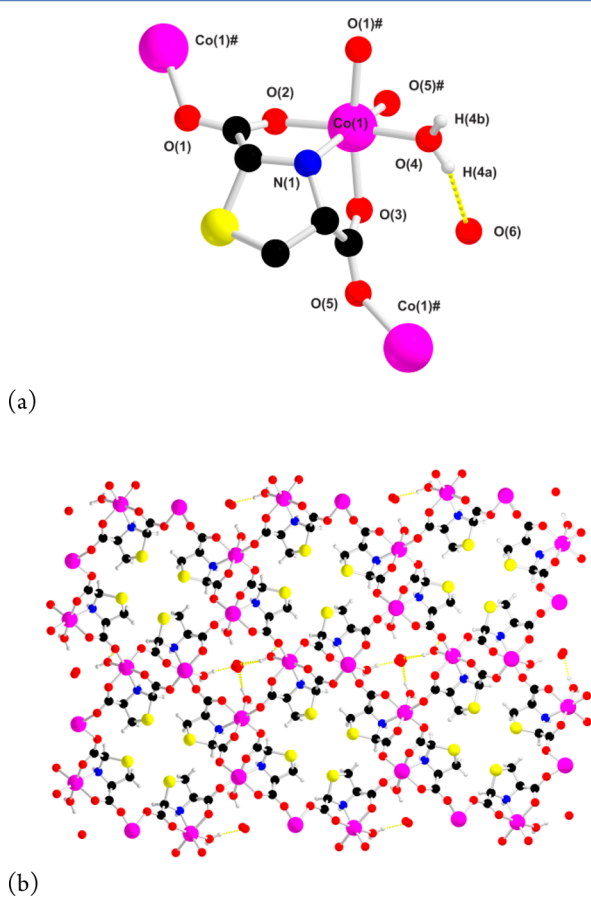

(a)

(b)

Figure 1. Cobalt coordination sphere (a) and 3D network (b) of 1.

water molecule that can be removed upon thermal treatment of the as-synthesized material at 190 °C for 24 h. The activated form $[Co(L\text{-}RR)]_\infty$ (1_{act}) maintains the same lattice structure as 1. In the present work, 1_{act} has been exploited as a heterogeneous catalyst for the oxidation of selected alkenes

under both anaerobic [tert-butyl hydroperoxide (^tBuOOH) as oxidant] and aerobic (O_2 as oxidant) conditions.

■ EXPERIMENTAL SECTION

General Considerations. All catalytic tests have been performed either under inert atmosphere in flame-dried flasks using standard Schlenk-type techniques or under O_2 atmosphere at variable pressures using a stainless steel autoclave (15 mL internal volume) equipped with a magnetic stirrer, a Teflon inset, a pressure controller, and a liquid/gas inlet. 1-Octene, cyclohexene, (Z)-cyclooctene and o-DCB (ortho-dichlorobenzene) were purified according to literature procedures[15] and stored over 4 Å molecular sieves under nitrogen. Unless otherwise stated, all other chemicals were purchased from commercial suppliers and were used as received without further purification. GC/MS analyses were performed on a Shimadzu QP2010S apparatus equipped with a flame ionization detector and a Supelco SPB-1 fused-silica capillary column (30 m length, 0.25 mm i.d., 0.25 μm film thickness). Chiral GC analyses were performed on a Shimadzu 17A apparatus equipped with a flame ionization detector and a Lipodex-E column (50 m length, 0.25 mm i.d., 0.25 μm film thickness).

General Procedure for the Catalytic Alkene Oxidation by 1_{act} Using ^tBuOOH As Oxidant. A mixture of the selected alkene (16 mmol), ^tBuOOH (8 mmol), and either o-DCB (used as internal standard for cyclohexene oxidation trials, 2 mmol) or 2,6-dimethylphenol (used as internal standard for 1-octene and (Z)-cyclooctene oxidation trials, 2 mmol) are added in one portion to the activated catalyst 1_{act} (0.095 mmol) weighed into a two-necked 25 mL flask.[16] The resulting suspension is stirred at 70 °C for 24 h. Afterward, the mixture is allowed to cool to room temperature, filtered over a Celite pad, and analyzed through gas chromatography. Catalyst recovery and recycling is operated under inert atmosphere by means of a careful removal of the supernatant and subsequent washing of the solid catalyst with dry and degassed n-pentane (5 mL). The solid residue is then left to dry under high vacuum for 1 h to remove all volatiles before resubmitting it for further oxidation cycles. Finally, hot filtration experiments were performed to confirm the heterogeneous nature of the catalyst, thus excluding any cobalt leaching from the activated MOF.

Catalytic Cyclohexene Oxidation by 1_{act} under Aerobic Conditions (O_2 As Oxidant). Compound 1_{act} (0.095 mmol) is weighed under inert atmosphere in a Teflon sample holder and placed in a 15 mL volume stainless steel autoclave equipped with a magnetic stirrer. The reactor is purged with three nitrogen—vacuum cycles and then filled with a solution of cyclohexene (16 mmol) and o-DCB (used as internal standard, 2 mmol). The reactor is then pressurized with oxygen at the desired pressure (1, 3, or 5 bar) and kept at 70 °C for 24 h. Oxygen is continuously fed to keep the reactor pressure constant throughout the catalytic test. After that time, the system is allowed to cool to room temperature, filtered over a Celite pad, and analyzed through gas chromatography. Catalyst recovering and recycling is operated following a procedure similar to that described above for catalysis using ^tBuOOH as oxidant.

TPD-MS Measurements. The TPD-MS analysis is performed through the Hiden Analytical CATLAB instrument (http://www.hidenanalytical.com) on sample 1_{act} pretreated with O_2 or ethylene at p = 5 bar in a closed vessel at 70 °C for 2 h. Thermal desorption on the pressurized samples is carried out under an argon flow (flow rate = 20 mL/min) in the 20−300

°C temperature range (sample heating rate = 5 °C/min). The quadrupole mass detector limit is 2×10^{-14} Torr.

Computational Details. Periodic DFT calculations were performed using the gradient-corrected Perdew−Burke−Ernzerhof (PBE) functional[17] as implemented in the VASP software package.[18] The long-range dispersion interactions were included using the PBE-D2 method based on Grimme's parameters.[19] The core electrons were described by the projector augmented wave (PAW) method.[20] In all of the VASP calculations, spins were polarized. For the cell and geometry relaxations, the systems were fully relaxed until the total energy was converged to 10^{-4} eV. The cell parameters were first calculated by optimizing the cell volume and atomic positions. The Co-MOFs with and without water on Co metal sites were optimized using unit cells with 80 atoms and 68 atoms, respectively. The energy cutoff was set at 800 eV, and a Monkhorst−Pack grid of $(2 \times 2 \times 2)$ was used.[21] For O_2 adsorption calculations, the lattice constants were fixed at the calculated value with Co open metal sites, and only atomic positions were allowed to relax using the energy cutoff of 400 eV. A $4 \times 4 \times 8$ k-point mesh was used. Atomic charges were obtained based on Bader charge analysis.[22] We also tested and optimized all geometries through a GGA(PBE)+U approach.[23] The self-interaction error in the 3d orbitals of Co was corrected, and 3.5 eV was used as the U_{eff} parameter.[24] Calculated adsorption energies were close to the GGA calculated values and are listed in the Supporting Information (SI). The oxygen adsorption energy of $\mathbf{1_{act}}$ was calculated on the basis of the equation $\Delta E_{ads} = E(MOF - O_2) - [E(MOF) + E(O_2)]$. For loadings higher than one molecule of O_2/cell, the *average* O_2 adsorption energies were calculated as follows: $\Delta E_{avg} = 1/n \times \{E(MOF - nO_2) - [E(MOF) + nE(O_2)]\}$. The *differential* O_2 adsorption energies were calculated through the simplified equation: $\Delta E_{diff} = E(MOF + nO_2) - \{E[MOF + (n - 1)O_2] + E(O_2)\}$.
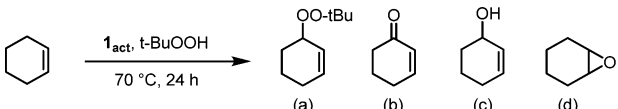
■ RESULTS AND DISCUSSION

Catalytic Alkene Oxidation by $\mathbf{1_{act}}$ Using ^tBuOOH As Oxidant. The activated chiral MOF $\mathbf{1_{act}}$ has been preliminarily scrutinized as a heterogeneous catalyst for the oxidation of selected alkenes (cyclohexene, (Z)-cyclooctene, 1-octene) using ^tBuOOH as oxidant. For the sake of comparison, substrates and experimental conditions used for the oxidation process have been chosen according to those reported in similar literature precedents.[12e−g] A blank reaction test carried out in the absence of $\mathbf{1_{act}}$ has also been used to elucidate the catalyst role in terms of process activity and selectivity. Because the material has only very small pores (pore limiting diameter of 3.96 Å, as calculated from the crystal structure),[14] it can be assumed that the catalytic transformations take place at the crystallites' outer surface only, without diffusion into the MOF 3D lattice.

The liquid-phase cyclohexene oxidation by $\mathbf{1_{act}}/^tBuOOH$ is a relatively fast process with fairly good catalyst activity, together with remarkable selectivity toward the *tert*-butyl-2-cyclohexenyl-1-peroxide product (**a**, Table 1). Notably, cyclohexene oxidation under the same experimental conditions but in the absence of the catalyst is almost negligible, with ~1.6% of substrate conversion after 24 h at 70 °C and a moderate catalyst selectivity (Table 1, entries 1 vs 2).

Using 0.095 mmol of $\mathbf{1_{act}}$ in the presence of a large excess of ^tBuOOH, the highest substrate conversion achieved after 24 h at 70 °C was 19.0%. The conversion obtained in this case is

Table 1. Cyclohexene Oxidation Catalyzed by $\mathbf{1_{act}}$ Using ^tBuOOH As Oxidant[a]

entry	$\mathbf{1_{act}}$ (mmol)	conv %[b,c]	a %[c]	b %[c]	c %[c]	d %[c]
1	0	1.6	58	23	19	
2	0.095	18.6	100[d]			
3[e]		19.0[f]	99	<1	<1	
4[g]	0.095	19.0	100			
5[h]	0.095	18.4	93	5	1	1
6[i]	0.095	16.7	92	5	1	2

[a]Oxidation conditions, ^tBuOOH (8 mmol); reaction temperature, 70 °C; reaction time, 24 h. [b]Calculated from the GC trace using o-DCB as internal standard. [c]Average values calculated over three independent runs. [d]ee, 24%. [e]Hot filtration test; reaction of the filtered supernatant deriving from entry 2 after additional 2 h at 70 °C. [f]Cobalt leaching measured by GF-AAS analysis ≈ 0.002%. [g]Catalyst recycling from entry 2 (2nd run). [h]Catalyst recycling from entry 4 (3rd run). [i]Catalyst recycling from entry 5 (4th run).

lower than those measured for MFU-1 (27% after 22 h),[12f] $[Co_3(BTC)_2(HCOO)_4(DMF)]\cdot H_2O$ (84% after 24 h),[12a] or MFU-3 (62% after 12 h)[12g] under similar experimental conditions; nonetheless, it is slightly higher than that of MFU-2 (16% after 22 h).[12e] As for chemoselectivity, when compared with the previous examples, $\mathbf{1_{act}}$ shows a higher selectivity toward a 100% conversion to the *tert*-butyl-2-cyclohexenyl-1-peroxide product, **a**. Indeed, only the 83% of product **a** was obtained with MFU-3 as catalyst, whereas 66% was the maximum amount of **a** that can be obtained from MFU-1 or MFU-2 under similar reaction conditions. The compound $[Co_3(BTC)_2(HCOO)_4(DMF)]\cdot H_2O$ gave a completely different selectivity toward the ketone, **b** (95% after 24 h). The peroxide (**a**) was the main oxidation product deriving from the cobalt-mediated allylic substitution on cyclohexene when ^tBuOOH was used as oxidant.[25] Thus, the proposed mechanism of cyclohexene conversion into **a** in the presence of ^tBuOOH (SI Scheme S2) is of the same kind as that reported for MFU-1.[12f] In line with this mechanistic hypothesis, 1 equiv of the byproduct ^tBuOH (in a 1:1 stoichiometric ratio with respect to **a**) was also observed on the GC traces of the reaction solutions. With the aim of excluding any possible contamination by homogeneous metal active sites responsible for the observed catalyst activity and selectivity (cobalt leaching), a hot filtration test and an ICP-MS analysis of the metal content in the supernatant were performed. Accordingly, the oxidation (Table 1, entry 2) was allowed to proceed for 24 h before being split into two fractions, one containing the suspended catalyst and the other filtered to remove any solid precipitate. The whole procedure was performed at 70 °C under inert atmosphere to prevent any oxygen contamination of both catalyst and solution. The solution was finally allowed to react for an additional 24 h at 70 °C before being analyzed via GC/MS (Table 1, entry 3).
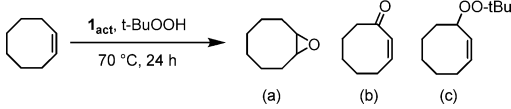
As can be inferred from the analysis of reaction products obtained from the resubmission of the filtered supernatant (entry 3), only a negligible increase in the substrate conversion was observed, and new oxidation products [namely, traces of 2-cyclohexen-1-one (**b**) and 2-cyclohexen-1-ol (**c**)] started to appear. The slight conversion increase (~0.4%; Table 1, entries

2 vs 3) is reasonably ascribed to the action of the excess of ^{t}BuOOH, whereas the role of homogeneous Co^{II} species can be definitely ruled out from the GF-AAS analysis of the cyclohexene solution at the end of the catalytic cycle (Table 1, entry 3). Indeed, a content of ≈0.002% of "leached" cobalt ions was detected in solution, thus labeling the process as truly heterogeneous in nature. In addition, product **a** from entry 2 showed a moderate enantiomeric excess (ee 24%) determined via chiral GC analysis of the reaction mixture;[26] this issue is in line with the chiral nature of the employed Co-MOF catalyst. To the best of our knowledge, this is the first example of a heterogeneous alkene oxidation performed with an optically pure Co-MOF catalyst. On the other hand, a racemic mixture (50:50) of the two (*R,S*) isomers of **a** was obtained in the absence of the catalyst (Table 1, entry 1).

Catalyst recovery and recycling was straightforwardly performed through complete solvent removal at the end of the first catalytic cycle. The solid residue was then rinsed with freshly distilled and degassed *n*-pentane (1 × 5 mL), filtered, and dried at room temperature under vacuum before being treated with an additional amount of cyclohexene and ^{t}BuOOH. This procedure was repeated under inert atmosphere at the end of each catalytic cycle. Compound **1**$_{act}$ maintained its catalytic activity almost unchanged during three successive oxidation cycles (Table 1, entries 2 vs 4–6), whereas a slight reduction of the catalyst selectivity became appreciable from the second catalyst recycling (Table 1, entries 2 and 4 vs 5). The contamination from secondary oxidation products (**b**–**d**) in the recycling runs is ascribed to the successive additions of a large excess of the oxidant, and the slightly reduced catalyst activity during the recycling is tentatively ascribed to its progressive deactivation caused by either adventitious moisture or catalyst loss.

The oxidation protocol was applied to another model cyclic olefin, (*Z*)-cyclooctene. Catalytic results are listed in Table 2.

Table 2. (Z)-Cyclooctene Oxidation Catalyzed by 1$_{act}$ Using ^{t}BuOOH As Oxidant^a

entry	**1**$_{act}$ (mmol)	conv %^{b,c}	**a** %^{c}	**b** %^{c}	**c** %^{c}
1	0	2.1	49	5	46
2	0.095	27.6	41	8	51
3^d	0.095	25.2	45	4	43
4^e	0.095	26.1	49	5	46

^{a}Oxidation conditions, ^{t}BuOOH (8 mmol); reaction temperature, 70 °C; reaction time, 24 h. ^{b}Calculated from the GC trace using 2,6-dimethylphenol as internal standard. ^{c}Average values calculated over three independent runs. ^{d}Catalyst recycling from entry 2 (2nd run). ^{e}Catalyst recycling from entry 3 (3rd run).

According to the procedure outlined above, a blank reaction test carried out in the absence of **1**$_{act}$ again was used to establish the role of the catalyst in terms of activity and selectivity.

As reported in Table 2, cyclooctene oxidation generally proceeds with higher substrate conversions (up to 28% after 24 h at 70 °C) but with a reduced selectivity compared with cyclohexene. A slightly higher percentage of the oxidation products was also observed in the blank test. The total conversion obtained in this reaction was lower than that
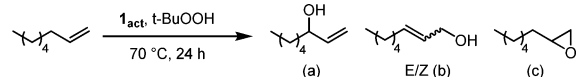
observed on the catalyst [Co$_3$(BTC)$_2$(HCOO)$_4$(DMF)]·H$_2$O (64%)[12a] under similar reaction conditions. Most importantly, the catalytic process led to mixtures of oxidation products in which the epoxide (**a**) and the *tert*-butyl-2-cyclooctenyl-1-peroxide (**c**) constitute ~90% of the mixture. Only a minor component (<10%) ascribed to the cyclooct-2-enone (**b**) was detected from the GC trace.

As for the process selectivity, the two main oxidation products (**a** and **c**) were obtained in nearly equal amounts. Although the epoxidation of (*Z*)-cyclooctene is expected to be the most favored process (allylic functionalization is more difficult than for other cycloalkenes, because of almost orthogonal allylic C–H bonds),[27] allylic oxidation still represents one important oxidation path under the experimental conditions used. Only a small fraction of 2-cyclooocten-1-one (up to 8%) was detected in the mixtures. Compound **1**$_{act}$ is also less selective than [Co$_3$(BTC)$_2$(HCOO)$_4$(DMF)]·H$_2$O, for which a selectivity of 78% toward the epoxide (**a**) was recorded.[12a]

Catalyst recycling was also performed on the cyclooctene oxidation trials, following the same experimental approach. Again, **1**$_{act}$ maintained its catalytic activity and selectivity unchanged for (at least) two successive oxidation cycles, (Table 2, entries 2 vs 3 and 4).

For the sake of completeness, 1-octene was finally selected as a model linear olefin for the catalytic oxidation tests. The experimental conditions used were the same as those applied to cyclic olefins, and catalytic outcomes are summarized in Table 3. 1-Octene oxidation proceeded with overall substrate

Table 3. 1-Octene Oxidation Catalyzed by 1$_{act}$ using ^{t}BuOOH As Oxidant^a

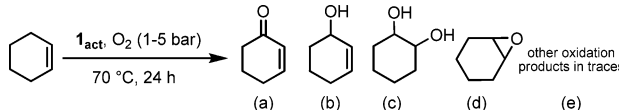| entry	**1**$_{act}$ (mmol)	conv %^{b,c}	**a** %^{c}	**b** %^{c}	**c** %^{c}
1	0	1.1	50	50	
2	0.095	18.8^d	37^e	52	11
3^f	0.095	17.3	35	53	12
4^g	0.095	17.9	35	57	8

^{a}Oxidation conditions, ^{t}BuOOH (8 mmol); reaction temperature, 70 °C; reaction time, 24 h. ^{b}Calculated from the GC trace using 2,6-dimethylphenol as internal standard. ^{c}Average values calculated over three independent runs. ^{d}Cobalt leaching measured by GF-AAS analysis ≈ 0.003%. ^{e}ee 18%. ^{f}Catalyst recycling from entry 2 (2nd run). ^{g}Catalyst recycling from entry 3 (3rd run).

conversions up to 19% after 24 h at 70 °C, with the production of mixtures made of three different oxidation products: oct-1-en-3-ol (**a**), (*E/Z*)-oct-2-en-1-ol (**b**) and the 2-hexyloxirane (**c**), the first two components representing about 90% of the mixture. Similarly to cyclohexene oxidation, the epoxidation product represents the minor component in the mixture. As can be argued from the product distribution, the allylic oxidation mechanism, proceeding via αH-abstraction and generation of an allylic radical, seems to be the main operating oxidation path in the process. Accordingly, the allylic substitution generated the two allylic alcohols with a branched to linear ratio of ~0.7. Substrate conversion and selectivity were almost completely preserved in the two successive oxidation cycles in which **1**$_{act}$ was recovered and reused according to the operative conditions used for the previously discussed oxidations on cyclic olefins.

The action of leached homogeneous Co^{II} species was definitively ruled out from the GF-AAS analysis of the crude reaction mixture at the end of the catalytic cycle (Table 3, entry 2). A content of ≈0.003% of "leached" cobalt ions was detected in the solution, thus confirming a truly heterogeneous process. In addition, a modest enantiomeric excess (ee 18%) was measured via chiral GC analysis on product **a** only; such a result confirms the (even moderate) induction ability of the enantiomerically pure cobalt coordination environment.

Catalytic Cyclohexene Oxidation by 1_{act} Using Molecular O_2 As Oxidant. To make a step forward in the oxidation of cyclic olefins, the activated chiral MOF 1_{act} has also been used under aerobic conditions, using molecular oxygen as oxidant. At odds with previously reported data on the aerobic oxidation of cyclic olefins,[12d,f,28] 1_{act} is capable of catalyzing cyclohexene oxidation efficiently without the employment of cocatalysts acting as electron-transfer mediators. As a matter of fact, cyclohexene conversions up to 37% were obtained after 24 h at 70 °C under constant O_2 pressure (Table 4, entry 3),

Table 4. Cyclohexene Oxidation Catalyzed by 1_{act} Using Molecular O_2 As Oxidant[a]

entry	1_{act} (mmol)	$p(O_2)$ (bar)	conv %[b,c]	a %[c]	b %[c]	c %[c]	d %[c]	e %[c]
1	0	2						
2	0.095	1	27.7[d]	54	29	7	1	9
3	0.095	2	36.7	49	29	11		11
4	0.095	3	33.9	43	17	23		17
5	0.095	5	20.3	59	22	9		10
6[e]	0.095	2	31.2	51	29	7		13
7[f]	0.095	2	32.6	54	26	9	2	9

[a]Oxidation conditions: O_2 (1–5 bar); reaction temperature, 70 °C; reaction time, 24h. [b]Calculated from the GC trace using o-DCB as internal standard. [c]Average values calculated over three independent runs. [d]Cobalt leaching measured by GF-AAS analysis ≈0.005%. [e]Catalyst recycling from entry 3 (2nd run). [f]Catalyst recycling from entry 6 (3rd run).

whereas no substrate conversion was shown when the reaction was carried out in the absence of the catalyst (Table 4, entry 1). The achieved conversion is the highest reported to date for this reaction catalyzed by Co(II) MOFs. MFU-1 showed a 35% conversion after 24 h at $T = 35$ °C in the presence of the radical initiator N-hydroxyphtalimide (NHPI),[12f] whereas almost 33% after 20 h was obtained with $[Co_2(DOBDC)(H_2O)_2]\cdot8H_2O$ (DOBDC = 2,5-dihydroxyterephthalate) under similar reaction conditions to ours.[12a] Higher conversions were recorded only for Fe(II)-containing MOFs, such as Fe-MIL-101 (up to 44% after 16 h), even if in this case a small amount of ^tBuOOH was added to the reaction mixture to initiate the process.

The aerobic oxidation protocol exhibited only moderate selectivity: indeed, five oxidation products have been detected, whose identity has been unambiguously assigned, together with small amounts of other unidentified oxidation byproducts (Table 4, e). The complete mass balance and substrate conversion were obtained from GC analysis of the crude reaction mixtures using o-DCB as internal standard. In the presence of radical initiators such as NHPI or ^tBuOOH, the

chemical selectivity is completely different, the main oxidation product being 2-cyclohexenyl-1-peroxide (not observed in our catalytic trials).[8,12f] In the absence of radical initiators, the two main products are the ketone (**a**) and the alcohol (**b**) in 78% and 90% total selectivity for 1_{act} and $[Co_2(DOBDC)(H_2O)_2]\cdot8H_2O$,[12d] respectively.

With the assumption that Co^{III}-superoxo species are responsible for the observed catalytic activity (vide infra and SI) and in the absence of electron-transfer cocatalysts, the process selectivity confirms the coexistence of two oxidation paths: epoxidation and allylic oxidation.[27] Although epoxide **d** and diol **c** are supposed to be generated from an epoxidation mechanism followed by an overoxidation of the epoxide to diol and regeneration of the pristine Co^{II} species (SI Scheme S1, eqs 2 and 5), a mechanism initiated by a substrate αH-abstraction with generation of an allylic radical can be reasonably invoked to justify the production of the allylic alcohol **b** (SI Scheme S1, eq 3). The major mixture component (**a**) is ultimately ascribed to an overoxidation path of the intermediate allylic alcohol **b** (SI Scheme S1, eq 4). The absence of exogenous sacrificial reductants (such as DMF) capable of promoting the regeneration of the pristine Co^{II} species[28] is apparently balanced by a substrate overoxidation (SI Scheme S1, eqs 3 and 5). Nevertheless, additional data and a more detailed mechanistic study (which are beyond the scope of the present work) are needed to provide unambiguous evidence for all the postulated intermediates.

Oxygen is continuously fed to the reactor to keep the desired pressure constant throughout the catalytic test. Although no appreciable variation of the product distribution is observed when the oxidation process is performed at increasing O_2 pressures, substrate conversions follow a more precise trend, reaching a maximum value for $pO_2 = 2$ bar. Thus, higher O_2 pressures (>2 bar) translates into a *reduced* substrate conversion. Such a trend may be ascribed to the "saturation" of all the exposed catalytic sites at pO_2 around 2 bar. On a speculative ground, the observed reaction trend could also be ascribed to the generation of binuclear Co-peroxo species forming at higher O_2 pressures between exposed metal ions at spatially close crystallite edges (SI Scheme S1, eq 1).[28a,29]

Catalyst recycling in successive oxidation tests has also been accomplished for catalysis performed under aerobic conditions. Thus, the catalyst is recovered at the end of the first oxidation cycle by cooling and depressurizing the reactor, decanting the solid catalyst, and removing the supernatant solution via a Teflon cannula under an O_2 flow. The solid catalyst is dried under a stream of O_2 before being rinsed with an additional amount of cyclohexene and repressurized at the desired O_2 pressure. As Table 4 shows, 1_{act} maintains its catalytic activity and selectivity almost unvaried for two successive oxidation cycles, the small conversion decrease being attributed to either a partial catalyst removal during the recovery procedure or catalyst poisoning by adventitious moisture (Table 4, entries 3 vs 6 and 7).

Temperature-Programmed Desorption of O_2 and Ethylene on 1_{act}. To assess the effective interaction of dioxygen with the heterogeneous catalyst and to verify if olefin coordination could also take place during the process, TPD-MS experiments were carried out on 1_{act} pretreated under O_2 or ethylene (as gaseous olefin model compound) under the same experimental conditions used for the catalytic trials. For dioxygen, the ion current vs temperature graphs for $m/z = 32$ a.m.u. (Figure 2) clearly indicate desorption of O_2, with a
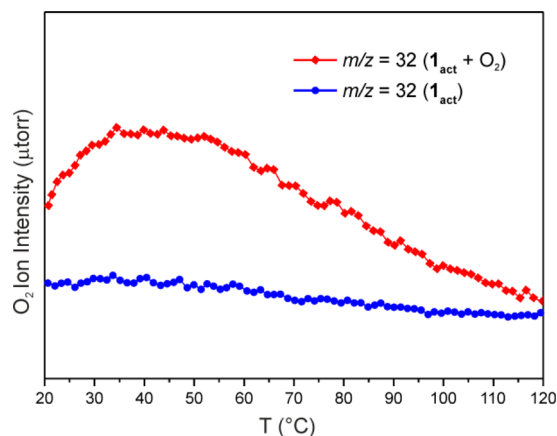
Figure 2. TPD-MS plot for O_2 desorption from 1_{act}.

maximum centered around 37 °C. The estimated ΔH_{des} at the curve maximum (inferred through the TPD Plotter integrated software[30]) equals 85.4 kJ/mol, in good agreement with the value coming from the computational results for the uptake of one O_2 molecule per unit cell (vide infra). The same experiments performed with ethylene (m/z = 26 and 27 a.m.u., SI Figure S1) revealed that no significant interaction between 1_{act} and the C=C bond occurs, the two TPD profiles being identical for the blank sample and that pretreated with ethylene. This may be due to the fact that the kinetic diameter of ethylene (4.5 Å) is slightly bigger than the MOF crystallographic pore size (3.96 Å, see above), thus preventing any chemical interaction between the olefin and the metal sites.

DFT Analysis of O_2 Uptake by 1_{act}. To get insight about how 1_{act} can activate O_2, we modeled the system through periodic DFT calculations. In the calculations, the interactions between O_2 and the cobalt sites in 1_{act} have been investigated. As noted above, the catalysis probably occurs on the outer surfaces of the MOF crystallites; however, given our lack of information about these sites, the interior open metal sites are a useful model for a preliminary understanding of O_2 activation in this system. In addition, the TPD measurements likely probe both inner and outer metal sites, since the kinetic diameter of O_2 (3.46 Å)[31] is slightly smaller than the pore limiting diameter of the MOF (3.96 Å). Consequently, it is reasonable to think that a partial O_2 diffusion through the particles outmost crystal layers occurs.

A cell size and geometry optimization was initially performed to obtain optimal lattice constants and structures of **1** and 1_{act}. The experimental X-ray structure was used as an initial guess. The lattice parameters calculated for **1** were very close to the experimental data, as shown in SI Table S1. During the geometry optimization, both **1** and 1_{act} had 12 unpaired electrons within a cell (three on each Co atom), which implies that Co^{2+} sites are in a high spin state. In this state, the 3D lattice can have different magnetic configurations. As shown in Figure 3, three different magnetic configurations were calculated. In the ferromagnetic configuration, all metal ions have the same spin states (Figure 3a), but in the other two possible antiferromagnetic configurations, neighboring metal ions have opposite spins (Figure 3b,c). Our results show that the antiferromagnetic configuration depicted in Figure 3b has the lowest total energy (ground state electronic energy), lower by 0.97 kJ/mol per Co atom than the ferromagnetic configuration (Figure 3a) and by 0.57 kJ/mol per Co atom
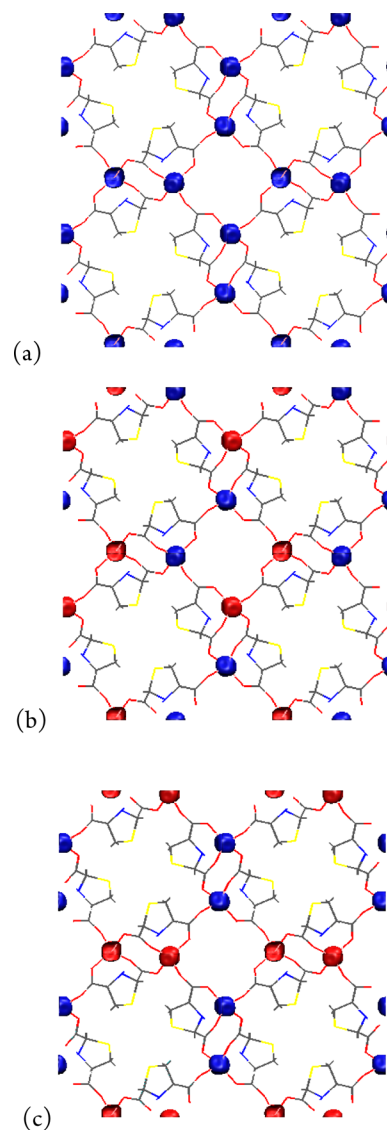

Figure 3. Magnetic configurations of the cobalt centers in 1_{act}: (a) ferromagnetic; (b, c) antiferromagnetic. The blue and red surfaces represent spin density surfaces with values of 0.3 and −0.3, respectively. The (2 × 2 × 1) extended cells are shown in the figure for better visualization.

than the other antiferromagnetic configuration (Figure 3c). This type of antiferromagnetic nature has also been shown to be the lowest energy configuration for other cobalt-containing MOFs, such as CPO-27-Co.[32]

For O_2 adsorption, the optimized geometry of 1_{act} was used. The cell parameters were kept constant (at the previously calculated value) throughout the calculation; only the atomic positions were allowed to relax. First, one oxygen molecule was introduced into the system, and the overall structure was fully optimized. Figure 4 shows the optimized geometry of O_2 adsorption on one Co site. The O−O bond length was elongated after adsorption from 1.235 Å (as found in free dioxygen) to 1.285 Å, showing a typical value of the superoxo-Co(III) fragment found in other literature examples (1.28 Å).[33] A Bader charge analysis was performed to investigate the charge distribution. Upon adsorption, the O_2 ligand gains charge from Co electronic back-donation; in addition, the coordinated oxygen atom bears a higher negative charge compared with the
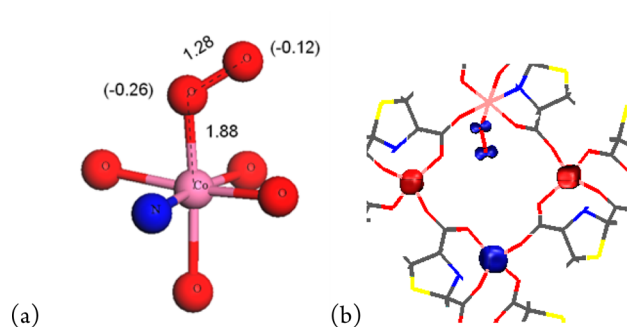
Figure 4. DFT-optimized geometry of one O_2 molecule/cell adsorbed by 1_{act}. (a) The coordination environment of the cobalt center after O_2 adsorption. The internuclear O−O and Co−O distances (Å) are reported. Atomic charges transferred to O atoms are reported in parentheses (see main text for details.) (b) The unpaired spin density surfaces in 1_{act} after O_2 adsorption. The blue and red isosurfaces represent 0.3 and −0.3, respectively.
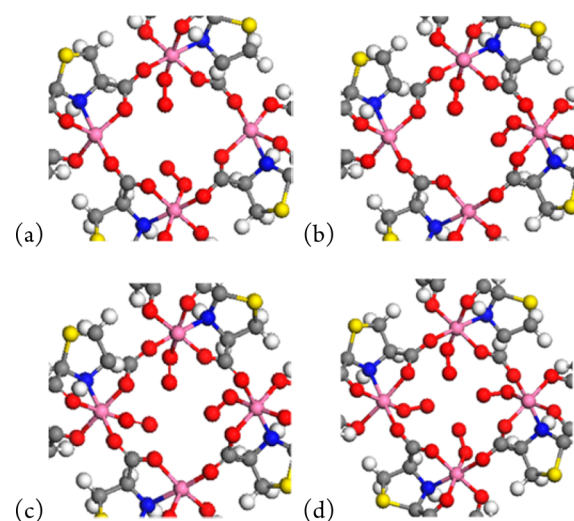

Figure 5. DFT optimized geometry of O_2 adsorption on 1_{act} at higher O_2 loadings. The geometry around the four Co centers is shown. (a) Two O_2 per unit cell adsorbed on opposite Co sites, (b) two O_2 per unit cell adsorbed on adjacent Co sites, (c) three O_2 per unit cell, and (d) four O_2 per unit cell.

distal oxygen atom, as shown in Figure 4a. The distribution of unpaired spin was also examined. After O_2 adsorption, the unpaired spin is localized mainly on the O_2 fragment, but not on the cobalt atom attached to it, which implies that, in the Co−O_2 adduct, the metal oxidation state is +3 (Co^{3+} = 3d^6), with all paired electrons. The crystal field splitting energy (Δ) of Co^{3+} is much larger than that of Co^{2+}, thus favoring a low spin state on Co^{3+}. According to crystal field theory, the splitting is also affected by the ligand strength. The superoxo (O_2^-) ligand is only slightly weaker than NH_3, again favoring a low spin configuration for the Co^{3+}−O_2^- fragment.[34]

The PBE-calculated O_2 adsorption energy on 1_{act} is −72 kJ/mol, and the (PBE+U)-calculated value is −75 kJ/mol. Higher loadings of O_2 were further analyzed by introducing more O_2 molecules into the computational model. For the adsorption of two oxygen molecules in the unit cell, two possible adsorption geometries were considered: the O_2 molecules on two *adjacent* Co sites and on two *opposite* Co sites. The latter was found to be slightly more stable ($\Delta\Delta E$ = 1 kJ/mol) at the computational level used (Table 5). For ΔE_{diff} related to three O_2 ligands/cell,

Table 5. O_2 Binding Energies^a on 1_{act} Calculated Using Periodic GGA Methods^b

coverage per unit cell	binding energy (kJ/mol)	
	av	differential
1 O_2	−72	
2 O_2 (opposite)	−71	−70
2 O_2 (adjacent)	−70	−68
3 O_2	−67	−58
4 O_2	−56	−25

^{a}In kJ/mol. ^{b}The corresponding values obtained with a periodic GGA +U approach are listed in Table S2.

the E[MOF + 2O_2] reference value was that of the geometry in which the two O_2 ligands were placed on opposite Co sites. The adsorption energy decreases for higher loadings, especially for a fully saturated loading (Figure 5 and Table 5). This can be attributed to a repulsive electrostatic effect.

■ CONCLUSIONS

The chiral Co(II) MOF $[Co(L\text{-}RR)(H_2O)\cdot H_2O]_\infty$ has been exploited for the catalytic oxidation of selected alkenes under

both anaerobic and aerobic conditions. Different activities and selectivities have been observed, together with a moderate chiral induction as measured on selected chiral oxidation products. The results using O_2 as the oxidant are consistent with a mechanism that proceeds through the generation of an η^1-superoxo species with no evidence for any significant interaction of the olefin with the metal center and its chiral environment. This is probably why only a moderate ee is observed for the analyzed chiral oxidation products. Among the various olefins considered, cyclohexene is the most efficiently oxidized substrate. During its anaerobic oxidation, a 100% selectivity toward the chiral *tert*-butyl-2-cyclohexenyl-1-peroxide product has been achieved, albeit with a moderate conversion (at *t* = 24 h). The highest conversion (37% after 24 h) reported to date for a Co-MOF catalyzed cyclohexene oxidation (but a lower selectivity) is achieved under aerobic conditions, leading to the α,β-unsaturated ketone 2-cyclohexenone as the main product. As a complement to the experimental work, a DFT computational analysis of O_2 interaction with the exposed metal sites in 1_{act} was performed. The optimized structures, the calculated atomic charges, and the spin state are consistent with the η^1-superoxo nature of bound O_2. The calculated adsorption energy of one O_2 molecule per unit cell is in good agreement with the value obtained experimentally from TPD-MS. Following these results, new thiazole-based MOFs containing exposed metal sites are currently being prepared in our laboratories for the study of new catalytic processes.

■ ASSOCIATED CONTENT

Ⓢ Supporting Information

Complementary DFT tables and Cartesian coordinates of the optimized geometries, hypothesized reaction schemes, TPD-MS results for ethylene. Additional experimental data (GC traces) are available from the authors on request. This material is available free of charge via the Internet at http://pubs.acs.org.

■ AUTHOR INFORMATION

Corresponding Author

*E-mail: a.rossin@iccom.cnr.it.

Notes

The authors declare no competing financial interest.

■ ACKNOWLEDGMENTS

■ REFERENCES

(1) (a) Zhao, D.; Timmons, D. J.; Yuan, D.; Zhou, H.-C. *Acc. Chem. Res.* **2011**, *44*, 123−133. (b) Chen, B.; Xiang, S.; Qian, G. *Acc. Chem. Res.* **2010**, *43*, 1115−1124. (c) Li, J.-R.; Kuppler, R. J.; Zhou, H.-C. *Chem. Soc. Rev.* **2009**, *38*, 1477−1504. (d) Britt, D.; Tranchemontagne, D.; Yaghi, O. M. *Proc. Natl. Acad. Sci. U.S.A.* **2008**, *105*, 11623−11627. (e) Mueller, U.; Schubert, M.; Teich, F.; Puetter, H.; Scherie-Arndt, K.; Pastré, J. *J. Mater. Chem.* **2006**, *16*, 626−636.

(2) (a) Li, J.-R.; Sculley, J.; Zhou, H.-C. *Chem. Rev.* **2012**, *112*, 869−932. (b) Li, J.-R.; Kuppler, R. J.; Zhou, H.-C. *Chem. Soc. Rev.* **2009**, *38*, 1477−1504.

(3) (a) Kreno, L. E.; Leong, K.; Farha, O. K.; Allendorf, M.; Van Duyne, R. P.; Hupp, J. T. *Chem. Rev.* **2012**, *112*, 1105−1125. (b) Shekhah, O.; Liu, J.; Fischer, R. A.; Woll, C. *Chem. Soc. Rev.* **2011**, *40*, 1081−1106.

(4) (a) Li, Y.-W.; Li, Y.-R.; Wang, L.-F.; Zhou, B.-Y.; Chen, Q.; Bu, X.-H. *J. Mater. Chem. A* **2013**, *1*, 495−499. (b) Jayaramulu, K.; Narayanan, R. P.; George, S. J.; Maji, T. K. *Inorg. Chem.* **2012**, *51*, 10089−10091. (c) Luo, F.; Batten, S. R. *Dalton Trans.* **2010**, *39*, 4485−4488.

(5) (a) Huxford, R. C.; Della Rocca, J.; Lin, W. *Curr. Opin. Chem. Biol.* **2010**, *14*, 262−268. (b) Keskin, S.; Kizilel, S. *Ind. Eng. Chem. Res.* **2011**, *50*, 1799−1812.

(6) (a) Dhakshinamoorthy, A.; Garcia, E. *Chem. Soc. Rev.* **2012**, *41*, 5262−5284. (b) Yoon, M.; Srirambalaji, R.; Kim, K. *Chem. Rev.* **2012**, *112*, 1196−1231. (c) Lillerud, K. P.; Olsbye, U.; Tilset, M. *Top. Catal.* **2010**, *53*, 859−868.

(7) Caron, S.; Dugger, R. W.; Ruggeri, S. G.; Ragan, J. A.; Ripin, D. H. B. *Chem. Rev.* **2006**, *106*, 2943−2989.

(8) Skobelev, I. Y.; Sorokin, A. B.; Kovalenko, K. A.; Fedin, V. P.; Kholdeeva, O. A. *J. Catal.* **2013**, *298*, 61−69.

(9) (a) Song, F.; Wang, C.; Falkowsky, J. M.; Ma, L.; Lin, W. *J. Am. Chem. Soc.* **2010**, *132*, 15390−15398. (b) Cho, S.; Ma, B.; Nguyen, S. T.; Hupp, J. T.; Albrecht-Schmitt, T. E. *Chem. Commun.* **2006**, 2563−2565.

(10) (a) Balu, A. M.; Lin, C.; Liu, H.; Li, Y.; Vargas, C.; Luque, R. *Appl. Catal., A* **2013**, *455*, 261−266. (b) Dhakshinamoorthy, A.; Alvaro, M.; Garcia, H. *J. Catal.* **2012**, *289*, 259−265.

(11) (a) Luz, I.; Léon, A.; Boronat, M.; Llabrés i Xamena, F. X.; Corma, A. *Catal. Sci. Technol.* **2013**, *3*, 371−379. (b) Brown, K.; Zolezzi, S.; Aguirre, P.; Venegas-Yazigi, D.; Paredes-Garcia, V.; Baggio, R.; Novak, M. A.; Spodine, E. *Dalton Trans.* **2009**, 1422−1427. (c) Wu, Y.; Qiu, L.; Wang, W.; Li, Z.; Xu, T.; Wu, Z.; Jiang, X. *Transition Met. Chem.* **2009**, *34*, 263−268.

(12) (a) Hamidipour, L.; Farzaneh, F. *React. Kinet. Mech. Catal.* **2013**, *109*, 67−75. (b) Zhang, J.; Biradar, A. V.; Pramanik, S.; Emge, T. J.; Asefa, T.; Li, J. *Chem. Commun.* **2012**, *48*, 6541−6543. (c) Beier, M. J.; Kleist, W.; Wharmby, M. T.; Kissner, R.; Kimmerle, B.; Wright, P. A.; Grunwaldt, J.-D.; Baiker, A. *Chem.—Eur. J.* **2012**, *18*, 887−898. (d) Fu, Y.; Sun, D.; Qin, M.; Huang, R.; Li, Z. *RSC Adv.* **2012**, *2*, 3309−3314. (e) Tonigold, M.; Lu, Y.; Mavrandonakis, A.; Puls, A.; Staudt, R.;

Möllmer, J.; Sauer, J.; Volkmer, D. *Chem.—Eur. J* **2011**, *17*, 8671−8695. (f) Tonigold, M.; Lu, Y.; Bredenkötter, B.; Rieger, B.; Bahnmüller, S.; Hitzbleck, J.; Langstein, G.; Volkmer, D. *Angew. Chem., Int. Ed.* **2009**, *48*, 7546−7550. (g) Lu, Y.; Tonigold, M.; Bredenkötter, B.; Volkmer, D.; Hitzbleck, J.; Langstein, G. *Z. Anorg. Allg. Chem.* **2008**, *634*, 2411−2417.

(13) Wang, C.; Liu, D.; Lin, W. *J. Am. Chem. Soc.* **2013**, *135*, 13222−13234.

(14) Rossin, A.; Di Credico, B.; Giambastiani, G.; Peruzzini, M.; Pescitelli, G.; Reginato, G.; Borfecchia, E.; Gianolio, D.; Lamberti, C.; Bordiga, S. *J. Mater. Chem.* **2012**, *22*, 10335−10344.

(15) Perrin, D. D.; Armarego, W. L. F.; Perrin, D. R. *Purification of Laboratory Chemicals*, 2nd ed.; Pergamon: Oxford, New York, 1980; Vol. 1.

(16) In the case of 2,6-dimethylphenol, the standard was added *after* the catalysis to avoid the inhibition of free radicals formation (and related conversion decrease) caused by the same phenol.

(17) Perdew, J.; Burke, K.; Ernzerhof, M. *Phys. Rev. Lett.* **1996**, *77*, 3865−3868.

(18) (a) Kresse, G.; Furthmüller, J. *Comput. Mater. Sci.* **1996**, *6*, 15−50. (b) Kresse, G.; Furthmüller, J. *Phys. Rev. B* **1996**, *54*, 11169−11186.

(19) Grimme, S. *J. Comput. Chem.* **2006**, *27*, 1787−1799.

(20) Kresse, G.; Joubert, D. *Phys. Rev. B* **1999**, *59*, 11−19.

(21) Monkhorst, H. J.; Pack, J. D. *Phys. Rev. B* **1976**, *13*, 5188−5192.

(22) Sanville, E.; Kenny, S. D.; Smith, R.; Henkelman, G. *J. Comput. Chem.* **2007**, *28*, 899−908.

(23) Dudarev, S. L.; Botton, G. A.; Savrasov, S. Y.; Humphreys, C. J.; Sutton, A. P. *Phys. Rev. B* **1998**, *57*, 1505−1509.

(24) Wang, L.; Maxisch, T.; Ceder, G. *Phys. Rev. B* **2006**, *73*, 195107.

(25) Koola, J. D.; Kochi, J. K. *J. Org. Chem.* **1987**, *52*, 4545−4553.

(26) The absolute structure (*R* or *S*) of the main enantiomer was not determined.

(27) Neuenschwander, U.; Hermans, I. *J. Org. Chem.* **2011**, *76*, 10236−10240.

(28) (a) Quek, X.-Y.; Tang, Q.; Hu, S.; Yang, Y. *Appl. Catal., A* **2009**, *361*, 130−136. (b) Zhang, X.; Zeng, C.; Zhang, L.; Xu, N. *Kinet. Catal.* **2009**, *50*, 199−204. (c) Lu, X. H.; Xia, Q. H.; Fang, S. Y.; Xie, B.; Qi, B.; Tang, Z. R. *Catal. Lett.* **2009**, *131*, 517−525. (d) Salavati-Niasari, M.; Abdolmohammadi, S.; Oftadeh, M. *J. Coord. Chem.* **2008**, *61*, 2837−2851. (e) Jiang, J.; Li, R.; Wang, H.; Zheng, Y.; Chen, H.; Ma, J. *Catal. Lett.* **2008**, *120*, 221−228. (f) Jinka, K. M.; Sebastian, J.; Jasra, R. V. *J. Mol. Catal. A: Chem.* **2007**, *274*, 33−41. (g) Patil, M. V.; Yadav, M. K.; Jasra, R. V. *J. Mol. Catal. A: Chem.* **2007**, *277*, 72−80. (h) Kantam, M. L.; Rao, B. P. C.; Reddy, R. S.; Sekhar, N. S.; Sreedhar, B.; Choudary, B. M. *J. Mol. Catal. A: Chem.* **2007**, *272*, 1−5. (i) Tang, Q. H.; Zhang, Q. H.; Wu, H. L.; Wang, Y. *J. Catal.* **2005**, *230*, 384−397. (j) Tang, Q. H.; Wang, Y.; Liang, J.; Wang, P.; Zhang, Q. H.; Wan, H. L. *Chem. Commun.* **2004**, 440−441.

(29) Holleman, A. F.; Wiberg, E. *Lehrbuch der Anorganischen Chemie*, 101st ed.; De Gruyter: Berlin, New York, 1995.

(30) Waugh, K. C. *Appl. Catal.* **1988**, *43*, 315.

(31) Breck, D. W. *Zeolite Molecular Sieves*; John Wiley & Sons: New York, 1974, p 636.

(32) Yu, D.; Yazaydin, A. O.; Lane, J. R.; Dietzel, P. D. C.; Snurr, R. Q. *Chem. Sci.* **2013**, *4*, 3544−3556.

(33) (a) Bloch, E. D.; Murray, L. J.; Queen, W. L.; Chavan, S.; Maximoff, S. N.; Bigi, J. P.; Krishna, R.; Peterson, V. K.; Grandjean, F.; Long, G. J.; Smit, B.; Bordiga, S.; Brown, C. M.; Long, J. R. *J. Am. Chem. Soc.* **2011**, *133*, 14814−14822. (b) Greenwood, N. N.; Earnshaw, A. *Chemistry of the Elements*, 2nd ed.; Butterworth Heinemann: Burlington, MA, 2002, pp 604−616,

(34) Miskowski, V. M.; Robbins, J. L.; Treitel, I. M.; Gray, H. B. *Inorg. Chem.* **1975**, *14*, 2318−2321.